

FIG. 3 Magnetic-field dependence of the electronic specific heat of Pd⁵. For low applied fields, $B < 0.1 \delta/\mu_B$, the data are in qualitative agreement with the QSE model described in the text. Owing to the limitations of the model, no quantitative agreement can be expected for fields in the tesla range. The theoretical curve for 3 T is therefore only shown as an indication of the behaviour in high fields. The dotted curve shows the prediction¹⁰ for the equal-level spacing model in zero field.

presence of internal fields due to interparticle magnetic interactions, in particular for Pd⁵ (below 0.2 K).

We are convinced that quantum-size effects in an ensemble of even-odd electron particles provide the only possible explanation for our data. The theoretical curves shown in Figs 1–3 have been obtained using an extension²¹ of the QSE model calculations¹⁰. Since in our experiments on Pd we are in the limit of weak field and weak spin-orbit coupling, we adopt the orthogonal distribution for the level separations between E_F and the two nearest higher levels. All other levels are taken as equidistant in order to minimize the time needed for the numerical computations. This approximation should be quite reasonable¹⁰, as at low temperature only these few levels are populated, whereas at high temperatures ($T \gg \delta/k_B$) the details of the level distribution become irrelevant. The fits were made assuming an equal number of odd- and even-electron particles. For both χ_{el} and C_{el} they agree to an average level separation δ/k_B of 12 ± 1 K, 5 ± 1 K and 2.5 ± 1.5 K for Pd⁵, Pd⁷ and Pd⁸, respectively. We stress that both the susceptibility and specific-heat data may be fitted within the errors by the same values for δ , which is the only fitting parameter in the QSE model. (That the values of δ obtained do not scale fully with the volumes of the particles is attributed to the above-mentioned surface effects on the DOS at E_F .) For Pd_{coll} the δ value obtained (0.06 ± 0.02 K) is already so small that it could only be derived from the specific heat. It is of interest that the δ values are rather close to those obtained from the simple formula $4E_F/3N$, where N is the number of valence electrons in the cluster. With 10 electrons per Pd atom, and $E_F = 6.8$ eV, we obtain δ/k_B values of 19 K, 7.5 K, 5 K and 0.08 K for Pd⁵, Pd⁷, Pd⁸ and Pd_{coll}.

The trends in the experimental data appear to match well the predictions of the model. In particular the T^2 -dependence of C_{el} predicted for the orthogonal ensemble in the QSE regime, agrees well with the data on Pd⁵. The latter clearly rule out the equal-level-spacing model, which predicts exponential decay of C_{el} for $T \rightarrow 0$ (Fig. 3). The observed T^2 -dependence is to our knowledge the first experimental evidence for the presence of level-repulsion in metal particles. Also, the field-dependent phenomena seen for Pd⁵ appear to be qualitatively reproduced, given the limitations of the model, in which the orthogonal distribution is restricted to the two levels closest above E_F . Accordingly, in an applied field the model will start to fail as soon as the Zeeman splitting becomes comparable to δ (that is, for fields exceeding a few tesla). □

Received 19 July; accepted 5 November 1996.

1. Perenboom, J. A. A., Wyder, P. & Meier, F. *Phys. Rep.* **78**, 173–292 (1981).
2. Halperin, W. P. *Rev. Mod. Phys.* **58**, 533–606 (1986).
3. van Wees, B. J. et al. *Phys. Rev. Lett.* **60**, 848–850 (1988).
4. Wharam, D. A. et al. *J. Phys. C* **21**, L209–L214 (1988).
5. Krans, J. V., van Ruitenbeek, J. M., Fisun, V. V., Yanson, I. K. & de Jongh, L. J. *Nature* **375**, 767–769 (1995).
6. Gorter, C. J., *Physica* **17**, 777–780 (1951).
7. Kubo, R. *J. Phys. Soc. J.* **17**, 975–986 (1962).
8. Ralph, D. C., Black, C. T. & Tinkham, M. *Phys. Rev. Lett.* **74**, 3241–3244 (1995).
9. Gor'kov, L. P. & Eliashberg, G. M. *Sov. Phys. JETP* **21**, 940–947 (1965).
10. Denton, R., Mühlischlegel, B. & Scalapino, D. J. *Phys. Rev. B* **7**, 3589–3607 (1973).
11. Schmid, G. (ed.) *Clusters and Colloids. From Theory to Applications* (VCH, Weinheim, 1994).
12. de Jongh, L. J. (ed.) *Physics and Chemistry of Metal Cluster Compounds* (Kluwer, Dordrecht, 1994).
13. Schmid, G., Morun, B. & Malm, J.-O. *Angew. Chem. Int. Edn Engl.* **28**, 778–780 (1989).
14. Schmid, G. *Polyhedron* **7**, 2321–2329 (1988).
15. Schmid, G. et al. *J. Am. Chem. Soc.* **115**, 2046–2048 (1993).
16. Vargaftik, M. N. et al. *J. Chem. Soc. Chem. Commun.* 937–939 (1985).
17. van Leeuwen, D. A. *Phys. Rev. Lett.* **73**, 1432–1435 (1994).
18. Mulder, F. M., Stegink, T. A., Thiel, R. C., de Jongh, L. J. & Schmid, G. *Nature* **367**, 716–718 (1994).
19. van Leeuwen, D. A., van Ruitenbeek, J. M., Schmid, G. & de Jongh, L. J. *Phys. Lett. A* **170**, 325–333 (1992).
20. Foner, S., Doclo, R. & McNiff, E. J. Jr. *J. Appl. Phys.* **39**, 551–552 (1968).
21. de Jongh, L. J. & Sinzig, J. in *Localized and Itinerant Molecular Magnetism: From Molecular Assemblies to the Devices* (eds Coronado, E., Delhaes, P., Gatteschi, D. & Miller, J. S.) (Kluwer, Dordrecht, in the press).

ACKNOWLEDGEMENTS. We thank H. B. Brom and J. M. van Ruitenbeek for their interest. This work was part of the research program of the Stichting voor Fundamenteel Onderzoek der Materie (FOM) which is supported by the Nederlandse Organisatie voor Wetenschappelijk Onderzoek (NWO). The support of the European Community under the HCM programme is acknowledged.

CORRESPONDENCE and requests for materials should be addressed to L.J.d.J.

Vegetation and soil feedbacks on the response of the African monsoon to orbital forcing in the early to middle Holocene

J. Kutzbach*, G. Bonan†, J. Foley* & S. P. Harrison‡

* Center for Climatic Research, University of Wisconsin-Madison, 1225 West Dayton Street, Madison, Wisconsin 53706, USA

† National Center for Atmospheric Research, PO Box 3000, Boulder, Colorado 80307-3000, USA

‡ Dynamic Palaeoclimatology, Lund University, Box 117, Lund, S-221 00, Sweden

FOSSIL pollen, ancient lake sediments and archaeological evidence from Africa indicate that the Sahel and Sahara regions were considerably wetter than today during the early to middle Holocene period, about 12,000 to 5,000 years ago^{1–4}. Vegetation associated with the modern Sahara/Sahel boundary was about 5° farther north, and there were more and larger lakes between 15 and 30° N. Simulations with climate models have shown that these wetter conditions were probably caused by changes in Earth's orbital parameters that increased the amplitude of the seasonal cycle of solar radiation in the Northern Hemisphere, enhanced the land–ocean temperature contrast, and thereby strengthened the African summer monsoon^{5–7}. However, these simulations underestimated the consequent monsoon enhancement as inferred from palaeorecords⁴. Here we use a climate model to show that changes in vegetation and soil may have increased the climate response to orbital forcing. We find that replacing today's orbital forcing with that of the mid-Holocene increases summer precipitation by 12% between 15 and 22° N. Replacing desert with grassland, and desert soil with more loamy soil, further enhances the summer precipitation (by 6 and 10% respectively), giving a total precipitation increase of 28%. When the simulated climate changes are applied to a biome model, vegetation becomes established north of the current Sahara/

Sahel boundary, thereby shrinking the area of the Sahara by 11% owing to orbital forcing alone, and by 20% owing to the combined influence of orbital forcing and the prescribed vegetation and soil changes. The inclusion of the vegetation and soil feedbacks thus brings the model simulations and palaeovegetation observations into closer agreement.

Studies with climate models suggest that major changes in vegetation can affect climate significantly: replacement of tundra by boreal forest causes warming^{8,9}, desertification^{10–12} and tropical deforestation^{13,14} cause drying. But could vegetation/soil feedbacks have enhanced the climatic response of monsoons to orbital forcing 9,000 to 6,000 years ago? A previous climate model experiment found that the response of precipitation to orbital forcing was increased by lowering the surface albedo of the Sahara from ~0.30 to ~0.25 to represent desert being replaced by grassland at 9,000 years ago². Whereas this study used a relatively low-resolution atmospheric model (5° latitude by 7.5° longitude, and 11 vertical levels) with a relatively simple land-surface model that characterized vegetation differences only in terms of differences of surface albedo, we use an atmospheric model of higher resolution (2.8° by 2.8° and 18 levels) and employ a land-surface model (LSM) with an explicit treatment of vegetation and soil processes^{15–17}. The atmospheric model is a modified version of the NCAR Community Climate Model version 2 (CCM2)^{18–20}. The LSM solves for the vegetation and ground temperatures that balance the surface energy budget, taking into account ecological differences among vegetation types (leaf and stem area, leaf optical properties, leaf dimensions, surface roughness, stomatal physiology, root profile) and hydraulic and thermal differences among soil types (porosity, hydraulic conductivity, matric potential, slope of retention curve, thermal conductivity, heat capacity, albedo).

We did four climate simulations: control (modern climate), R (changes in radiation at 6,000 years ago), RV (changes in radiation and vegetation) and RVS (changes in radiation, vegetation and soil). The atmospheric CO₂ concentration and the seasonal cycle of ocean surface temperature are prescribed at modern values in all four simulations. In R we change the Earth's orbital parameters from modern to 6,000 years ago: eccentricity from 0.167 to 0.187, axial tilt from 23.4° to 24.1°, and date of perihelion from early January to mid-September²¹. The change in the date of perihelion increases the amplitude of the seasonal cycle of Northern Hemisphere insolation by ~5%, leading to enhanced heating in northern summer–autumn and enhanced cooling in northern winter–spring. In RV we modify the vegetation in northern Africa between 15° N and 30° N from desert (100% bare ground) or semi-desert (10% shrub, 90% bare ground) (control and R) to grassland (80% grass, 20% bare ground). The northern limit of the prescribed grassland goes beyond the limit indicated by palaeobotanical evidence^{1–4} and was chosen to test the model's sensitivity to a large change². It would have been more accurate to prescribe a shrub/grass mixture rather than grassland, however the LSM does not include this category. The change to grassland increases the leaf and stem areas within the vegetated fraction, decreases the surface albedo slightly, modifies the sensible heat flux, and modifies the partitioning

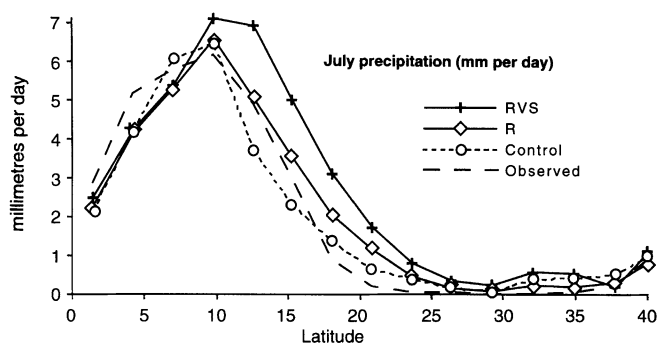


FIG. 1 July precipitation (mm per day) as a function of latitude and averaged longitudinally for the sector 0–50° E, for the control, experiment R and experiment RVS, and modern observations^{30,31}. Longitudinal averages are appropriate because the climate and vegetation of northern Africa are rather uniform longitudinally.

of the total latent heat flux into evaporation from soil, evaporation from vegetation, and transpiration. In RVS, we prescribe both the increased grassland and a more loamy soil to reflect the expected long-term increase in organic content of the soil under grassland. There is evidence of such a Holocene soil development from several locations in the Sahara^{22,23}. This change increases the available water capacity of the soil (from 0.22 m water per metre of soil in the control, R and RV to 0.24 m, an increase of ~10%) and decreases the rate at which the soil drains. Consistent with the higher organic content, we also change soil colour so that albedo decreases from 0.25 to 0.22 (Table 1).

Each of the simulations was run for 5.5 years. Systematic trends in soil moisture were small and generally similar in the four simulations after the first 1.5 years of spin-up and there were no discernible trends in other variables (such as temperature, precipitation). Although longer spin-up periods have been proposed²⁴, we believe that 1.5 years is adequate for these simulations. The control simulates July precipitation in good agreement with observations (Fig. 1).

Radiative forcing (R minus control) increases July insolation by ~20 W m⁻² (Fig. 2), leading to increases in net radiation at the

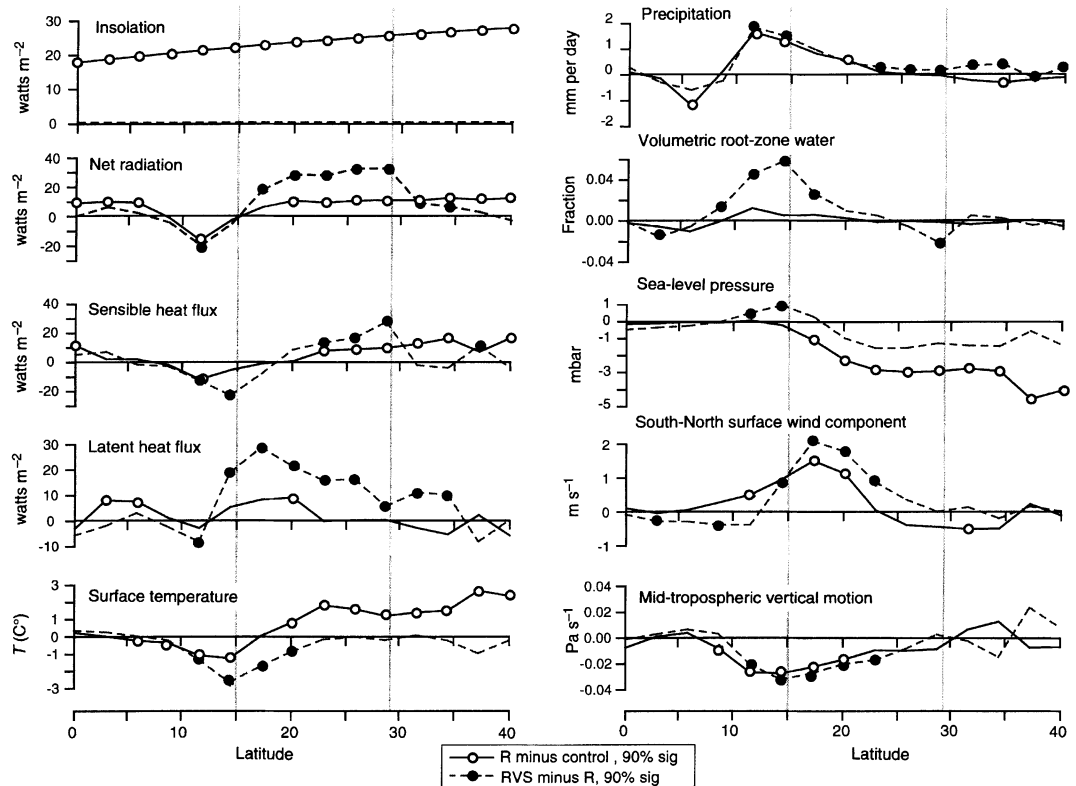
TABLE 1 Annual average climate, vegetation and soil variables for four simulations (15° N–22° N, 0–50° E)

Variable	Experiment			
	Control	R	RV	RVS
Insolation (top of atmosphere) (W m ⁻²)	399	398	398	398
Surface albedo (fraction)	0.25	0.25	0.25	0.22
Net surface radiation (W m ⁻²)	94	95	98	104
Sensible heat flux (W m ⁻²)	56	53	54	57
Evapotranspiration (W m ⁻²)	38	42	44	47
(Soil/canopy evaporation, W m ⁻²)	(35)	(39)	(35)	(39)
(Canopy transpiration, W m ⁻²)	(3)	(3)	(9)	(8)
Precipitation (mm per day)	1.28	1.43	1.51	1.63
Precipitation minus evapotranspiration (mm per day)	-0.03	-0.01	-0.02	0.00
Volumetric root-zone water (fraction)	0.18	0.18	0.18	0.20
Near-surface temperature* (°C)	28.7	27.5	27.3	27.5
Near-surface specific humidity* (g kg ⁻¹)	6.2	6.8	7.1	7.4
Total cloud (fraction)	0.33	0.37	0.36	0.37
Precipitation (15° N–22° N; fraction of control)	1.00	1.12	1.18	1.28
Precipitation (23° N–30° N; fraction of control)	1.00	0.99	0.96	1.13

R, radiation 6,000 years ago; RV, radiation and changed vegetation 6,000 years ago; RVS, radiation and changed vegetation and soils 6,000 years ago, averaged over the southern half of the region of modified vegetation/soil in RV and RVS (15° N–22° N, 0–50° E). The annual average is based on the final four years of simulation. At the bottom of the table, changes in precipitation (fraction) are shown, averaged over the southern and northern halves of the region of modified vegetation/soil. Values in bold denote that the differences R – control, RV – control, RVS – control are statistically significant at the 95% level.

* Near-surface refers to the lowest level of the model's atmosphere, 0.992σ; this corresponds roughly to a height of 50 m.

FIG. 2 Changes in simulated climatic conditions for July between experiment R and the control (solid lines), representing the response to orbital forcing, and between experiment RVS and experiment R (dashed lines), representing the response to vegetation/soil forcing; the changes are depicted as a function of latitude and are longitudinal averages, 0–50° E, averaged for the last four years of simulation. The symbols on each graph indicate that the change is significant at the 90% level (based on the *t*-test statistic of the difference in mean values compared to the model's own year-to-year variability). Vertical lines indicate the region of modified vegetation/soil in experiment RVS. In the chart illustrating surface winds, positive values indicate stronger southerly wind components. In the chart illustrating vertical motion, more upward motion is negative and 0.01 Pa s^{-1} corresponds to $\sim 1.5 \text{ mm s}^{-1}$.



surface ($\sim 10 \text{ W m}^{-2}$), in sensible heat flux ($\sim 10 \text{ W m}^{-2}$) and in surface temperature (~ 1 to 2°C north of 20°N). The enhanced monsoon circulation is indicated by decreased sea-level pressure (~ -2 to -3 mbar), increased southerly wind ($\sim 1 \text{ m s}^{-1}$) and increased mid-troposphere upward air motion (Fig. 2). Precipitation increases by 1–2 mm per day between 10°N and 20°N (Fig. 2), representing a 2° latitude northward extension of the summer monsoon (Fig. 1). In the region of enhanced rainfall, soil water increases slightly, evapotranspiration increases ($\sim 10 \text{ W m}^{-2}$) and cloudiness increases, leading to a decrease in temperature (about -1°C). The response of precipitation to orbital forcing in this version of CCM2 is substantially weaker than the response obtained previously with CCM1 (ref. 25), and also substantially less than is required to account for the observations of mid-Holocene moist environments. There are differences in both resolution and subgrid-scale parameterizations between these two models, so it is difficult to pinpoint the cause of their different climatologies and different monsoonal responses to orbital forcing^{26,27}.

Vegetation/soil forcing (RVS minus R) enhances the summer monsoon significantly compared to orbital forcing alone (Fig. 2). The climatic response to vegetation/soil forcing equals or exceeds the response to orbital forcing in magnitude, and both kinds of forcing produce similar changes with latitude. The surface net radiation increases by 25 W m^{-2} , latent heat flux (evapotranspiration) by $\sim 20 \text{ W m}^{-2}$, and soil water by more than 10%. There is additional lowering of sea-level pressure, increased southerly wind, and increased upward air motion (Fig. 2). The change in July precipitation, which is greatest over the southern half of the modified region, equals that due to orbital forcing alone (Fig. 2) and represents an additional 2° latitude northward extension of monsoon rains (Fig. 1). The change in July precipitation is statistically significant at most latitudes from 13°N to 40°N , and changes in other variables are statistically significant over more limited domains (Fig. 2). Whereas the orbitally induced enhancement of precipitation (R-control) occurs only in the period July–September, coincident with the maximum in orbital forcing, the enhance-

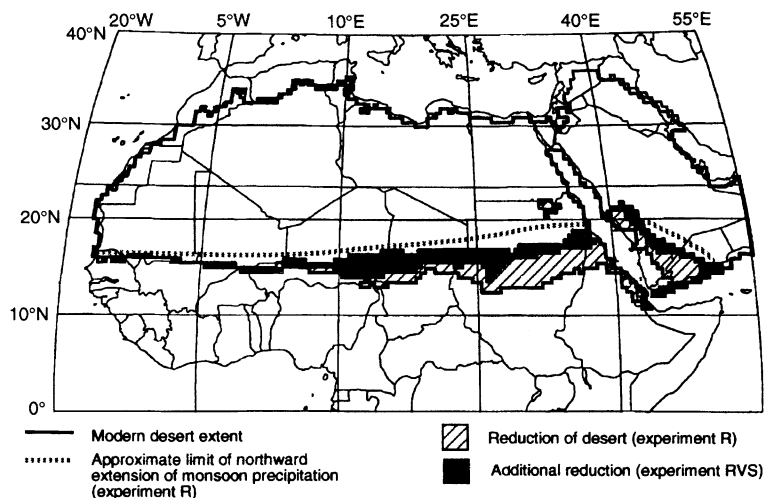
ment of precipitation due to vegetation/soil forcing (RVS minus R) occurs throughout the summer monsoon, May–September.

The hydrological response to vegetation/soil forcing is a strong function of the model's climate for the control and R. In the northern half of the modified region, 23°N – 30°N , precipitation is very low in the control and in R (Figs 1 and 2), and therefore the response of soil moisture and precipitation in RVS is small (Fig. 2). In the southern half of the modified region, 15°N – 22°N , where precipitation in the control exceeds 1 mm per day and where the response of precipitation in R is largest (Figs 1, 2), the response of the hydrological cycle to vegetation/soil forcing is considerable (Figs 1, 2).

Both the increased available water capacity of the soil and the decreased surface albedo in RVS, compared to RV, appear to be important. Root-zone soil water increases 10% in RVS, relative to RV, R and the control, and the model's evapotranspiration is sensitive to this increase (Table 1). The lowered surface albedo in RVS accounts for much of the increased net radiation between RVS and R (9 W m^{-2}); the corresponding increase between RV and R is only 3 W m^{-2} . This increase in available water and in net radiation in RVS, compared to R, helps drive the increased evapotranspiration (5 W m^{-2}) contributed by increased canopy transpiration; the corresponding increase between RV and R is only 2 W m^{-2} . In response to the increased evapotranspiration, near-surface specific humidity increases from 6.8 g kg^{-1} in R to 7.1 g kg^{-1} in RV to 7.4 g kg^{-1} in RVS. The increased humidity, low-level flow convergence, and upward vertical motion (Fig. 2) combine to enhance precipitation: R, 12% increase, RV, 18% increase, RVS, 28% increase, all compared to the control (Table 1).

Could the prescribed vegetation/soil changes have increased precipitation sufficiently in the southern half of the region to be self-maintaining? We begin to address this question by forcing a physiologically based biome model²⁸ with the output from the climate model. The four-year simulations are too short to provide an accurate climatology for the biome estimates, but nevertheless illustrate the direction of change. Compared to the modern

FIG. 3 Location of desert as simulated by a physiologically based biome model²⁸ driven by output from experiments R and RVS (mean monthly temperature, precipitation, solar radiation), compared to modern. The hatched line marks the approximate limit of northward extension of monsoon precipitation in experiment R. Slant hatching indicates the reduction in the area of desert in experiment R; dark shading indicates the additional reduction in experiment RVS. The shrinking desert is replaced by xerophytic woods/scrub and warm grass/shrub vegetation.



control, R produces a larger area of xerophytic woods/scrub and warm grass/shrub vegetation so that the desert area in the region 0–50° E, 0–30° N, is reduced by 11%; desert is reduced by 16% in RV and 20% in RVS (Fig. 3). The vegetation simulated by RVS is in better agreement with palaeovegetation than that simulated by R (refs 1–4), especially around Lake Chad and eastward into the Sudan where both the simulation and the palaeoenvironmental observations^{1–4} indicate vegetation 3° to 5° north of modern limits. None of the simulations produce vegetation in northwest Mali and northeast Sudan as indicated by observations^{1–4}. However, it is possible that the northernmost sites record local palaeovegetation rather than a broad continent-wide extension.

Our results and earlier studies^{2,7–17} suggest that climate models need to include biospheric processes involving both vegetation and soils. Other factors that might further enhance the climatic response to orbital forcing include the extensive lakes and marshes that existed in northern Africa in the middle Holocene (refs 1–4, and M. T. Coe, personal communication, and changes in ocean circulation that could influence sea surface temperatures. Our results also have implications for the accurate simulation of possible future climates. Climate models simulate changes in African monsoon precipitation in response to increased greenhouse gases²⁹, but these models will need to include possible vegetation and soil feedbacks to assess more accurately the magnitude of future climate change. □

28. Prentice, I. C. et al. *J. Biogeogr.* **19**, 117–134 (1992).

29. Mitchell, J. F. B., Manabe, S., Meleshko, V. & Tokioka, T. in *Climate Change: The IPCC Scientific Assessment* (eds Houghton, J. T., Jenkins, G. J. & Ephraums, J. J.) 131–172 (Cambridge Univ. Press, Cambridge, 1990).

30. Legates, D. R. & Willmott, C. *J. Theor. Appl. Climatol.* **41**, 11–21 (1990).

31. Legates, D. R. & Willmott, C. *J. Int. J. Climatol.* **10**, 111–127 (1990).

ACKNOWLEDGEMENTS. We thank P. Behling, R. Selin and J. Kruepke for assistance with model simulations and graphics, and M. Kennedy for preparing the manuscript. This research was supported by grants to the University of Wisconsin–Madison by the NSF Climate Dynamics Program, and the Department of Energy, by the National Center for Atmospheric Research, which is sponsored by the NSF, and by awards to Lund University from the European Community, the Swedish Natural Science Research Council, and the Craford Fund.

CORRESPONDENCE should be addressed to J. K. (e-mail: jek@facstaff.wisc.edu).

Leading-edge vortices in insect flight

Charles P. Ellington, Coen van den Berg*, Alexander P. Willmott* & Adrian L. R. Thomas*

Department of Zoology, University of Cambridge, Downing Street, Cambridge, CB2 3EJ, UK

INSECTS cannot fly, according to the conventional laws of aerodynamics: during flapping flight, their wings produce more lift than during steady motion at the same velocities and angles of attack^{1–5}. Measured instantaneous lift forces also show qualitative and quantitative disagreement with the forces predicted by conventional aerodynamic theories^{6–9}. The importance of high-lift aerodynamic mechanisms is now widely recognized but, except for the specialized fling mechanism used by some insect species^{1,10–13}, the source of extra lift remains unknown. We have now visualized the airflow around the wings of the hawkmoth *Manduca sexta* and a 'hovering' large mechanical model—the flapper. An intense leading-edge vortex was found on the downstroke, of sufficient strength to explain the high-lift forces. The vortex is created by dynamic stall, and not by the rotational lift mechanisms that have been postulated for insect flight^{14–16}. The vortex spirals out towards the wingtip with a spanwise velocity comparable to the flapping velocity. The three-dimensional flow is similar to the conical leading-edge vortex found on delta wings, with the spanwise flow stabilizing the vortex.

Several studies have visualized the airflow around flapping

Received 12 June; accepted 24 October 1996.

- Street, F. A. & Grove, A. T. *Nature* **261**, 385–390 (1976).
- Street-Perrott, F. A., Mitchell, J. F. B., Marchand, D. S. & Brunner, J. S. *Trans. R. Soc. Edinb.* **81**, 407–427 (1990).
- Petit-Maire, N. & Riser, J. *Palaeogeogr. Palaeoclimatol. Palaeoecol.* **35**, 45–61 (1981).
- Jolly, D., Harrison, S. P., Dammati, B. & Bonnefille, R. *Quat. Sci. Rev.* (in the press).
- Kutzbach, J. E. & Otto-Bliesner, B. L. *J. Atmos. Sci.* **39**, 1177–1188 (1982).
- Kutzbach, J. E. & Guetter, P. J. *J. Atmos. Sci.* **43**, 1726–1759 (1986).
- Mitchell, J. F. B., Grahame, N. S. & Needham, K. H. *J. Geophys. Res.* **93**, 8283–8303 (1988).
- Bonan, G. B., Pollard, D. & Thompson, S. L. *Nature* **359**, 716–718 (1992).
- Foley, J., Kutzbach, J. E., Coe, M. T. & Levis, S. *Nature* **371**, 52–54 (1994).
- Charnay, J. G., Quirk, W. J., Chow, S. H. & Kornfeld, J. *J. Atmos. Sci.* **34**, 1366–1385 (1977).
- Laval, K. & Picon, L. *J. Atmos. Sci.* **43**, 2418–2429 (1986).
- Xue, Y. & Shukla, J. *J. Clim.* **6**, 2232–2245 (1993).
- Henderson-Sellers, A. et al. *J. Geophys. Res.* **98**, 7289–7315 (1993).
- Nobre, C. A., Sellers, P. J. & Shukla, J. *J. Clim.* **4**, 957–988 (1991).
- Bonan, G. B. *J. Geophys. Res.* **99**, 25803–25818 (1994).
- Bonan, G. B. *J. Geophys. Res.* **100**, 2817–2831 (1995).
- Bonan, G. B. *J. Clim.* **8**, 2691–2704 (1995).
- Hack, J. J. et al. NCAR Technical Note TN-382+STR, 1–108 (National Center for Atmospheric Research, Boulder, CO, 1993).
- Hack, J. J., Boville, B. A., Kiehl, J. T., Rasch, P. J. & Williamson, D. L. *J. Geophys. Res.* **99**, 20785–20813 (1994).
- Kiehl, J. T. *J. Geophys. Res.* **99**, 23107–23115 (1994).
- Berger, A. *J. Atmos. Sci.* **35**, 2362–2367 (1978).
- Haynes, C. V. *Natl Geogr. Soc. Res. Rep.* **19**, 269–341 (1985).
- Petit-Maire, N. & Riser, J. *Sahara ou Sahel? Quatenaire récent du Bassin de Taoudenni (Mali)* (Lamy, Marseille, 1983).
- Milly, P. C. D. & Dunne, K. A. *J. Clim.* **7**, 506–526 (1994).
- Kutzbach, J. E. et al. *Quat. Sci. Rev.* (in the press).
- Sperber, K. R., Hameed, S., Potter, G. L. & Boyle, J. S. PCMDI Rep. No. 12, UCRL-ID-11532 (Lawrence Livermore National Laboratory, Livermore, CA, 1993).
- Boyle, J. S. *J. Clim.* **6**, 796–815 (1993).

* Present addresses: Faculty of Human Movement Sciences, Vrije Universiteit, Van der Boerhorststraat 9, 1081 BT Amsterdam, The Netherlands (C.v.d.B.); Kawachi Millibioflight Project, Japan Science and Technology Corporation (JST), Park Building 3F, 4-7-6 Komaba, Meguro-ku, Tokyo 153, Japan (A.P.W.); Department of Zoology, University of Oxford, South Parks Road, Oxford OX1 3PS, UK (A.L.R.T.).